energies

MDPI

Article

Optimization of Operating Conditions of a Solid Oxide Fuel Cell System with Anode Off-Gas Recirculation Using the Model-Based Sensitivity Analysis

Eun-Jung Choi [1], Sangseok Yu [2] and Sang-Min Lee [1,*]

[1] Department of Clean Fuel and Power Generation, Korea Institute of Machinery & Materials (KIMM), 156 Gajeongbuk-ro, Yuseong-gu, Daejeon 34103, Korea; ejchoi@kimm.re.kr

[2] School of Mechanical Engineering, Chungnam University, 99, Daehak-ro, Yuseong-gu, Daejeon 34134, Korea; sangseok@cnu.ac.kr

* Correspondence: victlee@kimm.re.kr; Tel.: +82-42-868-7833

Abstract: Designing a configuration of an efficient solid oxide fuel cell (SOFC) system and operating it under appropriate conditions are important for achieving a highly efficient SOFC system. In our previous research, the system layout of a SOFC system with anode off-gas recirculation was suggested, and the system performance was examined using a numerical model. In the present study, the system operating conditions were optimized based on the system configuration and numerical model developed in the previous paper. First, a parametric sensitivity analysis of the system performance was investigated to demonstrate the main operating parameters. Consequently, the fuel flow rate and recirculation ratio were selected. Then, the available operating conditions, which keep the system below the operating limits and satisfy the desired system performance (U_{fuel} > 0.7 and η_{elec} > 45%) were discovered. Finally, optimized operating conditions were suggested for three operating modes: optimized electrical efficiency, peak power, and heat generation. Depending on the situation, the demand for electricity and heat can be different, so different proper operating points are suggested for each mode. Additionally, using the developed model and the conducted process of this study, various optimized operating conditions can be derived for diverse cases.

Keywords: SOFC; anode off-gas recirculation (AOGR); hydrogen recirculation; SOFC simulation; sensitivity analysis

Citation: Choi, E.J.; Yu, S.; Lee, S.M. Optimization of Operating Conditions of a Solid Oxide Fuel Cell System with Anode Off-Gas Recirculation Using the Model-Based Sensitivity Analysis. *Energies* **2022**, *15*, 644. https://doi.org/10.3390/en15020644

Academic Editor: Orazio Barbera

Received: 20 December 2021
Accepted: 12 January 2022
Published: 17 January 2022

1. Introduction

Carbon-neutral technology issues have become a subject of special interest to cope with global climate change. Solid oxide fuel cells (SOFCs) have received great attention as low-emission power generation devices. They have diverse advantages such as high electrical efficiency, eco-friendliness, and fuel flexibility [1–3]. However, there are still some barriers to commercialization, such as low durability, high cost, and low reliability. To overcome these challenges, various reports have been published on improving system efficiency and finding control points that can ensure system safety [4,5].

An anode off-gas recirculation (AOGR) system can be adopted in the SOFC system as a method to enhance system performance. Generally, anode off-gas (AOG) contains 15–25% residual fuel; therefore, additional benefits of fuel utilization and electrical efficiency can be obtained by recycling AOG [1,6]. Several studies about SOFC systems with AOGR have been conducted. However, most of the studies suggested the effect of the AOGR system compared to the SOFC system without AOGR. System performance can be largely different depending on the system configurations. Therefore, in our previous paper [7], system performances with different system configurations were numerically examined. A survey of literature on SOFC systems with AOGR was conducted in the paper

[7]. Additional research papers [1,7–9] have been added to the previous literature survey and are summarized in Table 1.

Selecting the proper operating conditions and system configuration is also important for reliable system performance. The simulation model is widely used to determine the control algorithm and to optimize the operating point because of its cost-effectiveness. As various reactions in the SOFC system are complicated, simulation analysis is more effective in determining the cause-and-effect relationship of the system performance [4,10]. Many studies have conducted sensitivity analysis to determine the key operational and design parameters for a fuel cell system. For sensitivity analysis, a reliable model was first developed for the analysis object's system. Then, a parametric analysis was performed to evaluate the impact of diverse parameters on performance. The dominant parameter can be identified by comparing the sensitivity of each parameter [4,9–12]. Lee et al. [9] numerically examined a combined fuel reforming and SOFC system with AOGR with parametric sensitivity analysis and suggested an optimized point with the highest efficiency. Dhingra et al. [13] developed a model of a 1 kW diesel-fed SOFC system, which was studied using sensitivity analysis. Individual and paired variable sensitivities were examined to study the influence of the key operating variables on the system. The operating conditions of the steam-to-carbon (S/C) ratio, and the fuel and air utilization factor were suggested at the maximum efficiency point. A summary of the related papers bas been suggested in Table 2. Based on the numerical parametric analysis, the effects of system variables were examined in several papers. When the purpose of the study was to select design variables, the number of system variables was higher than others. Among them, two papers suggested the optimum operating condition for the maximum system efficiency.

Table 1. A literature summary of the solid oxide fuel cell (SOFC) system with anode off-gas recirculation (AOGR) (revised based on the Table 1 in ref. [7]).

Authors	SOFC Power	η_{ele} (Max.)	AOGR Device	Comments
Lee et al. [14]	5 kW	64.6%	Ejector	The turbocharger and ejector were used to blow cathode air and AOG. Sensitivity analysis was conducted to determine the optimal operating schemes.
Powell et al. [15]	1.7–2.2 kW	56.6% (LHV)	Blower	The system used an adiabatic external steam reformer and AOGR system. Heat and steam for steam methane reforming were provided by recirculated AOG.
Koo et al. [16]	113.8 kW	66% (LHV)	Blower	A cascade system with double SOFC system and single SOFC system with AOGR was analyzed using the exergy-based analysis method.
Wagner et al. [8,17]	6 kW	66% (LHV)	Fan	A novel micro AOGR fan was introduced and experimentally coupled to SOFC system.
Baba et al. [18]	1 kW	-	Ejector	SOFC system with a variable flow ejector was examined under partial load and full load conditions.
Tanaka et al. [19]	10 kW	58.7% (LHV)	Blower	AOGR blowers were developed and coupled with SOFC system simulator.
Dietrich et al. [20]	0.3 kW	41% (LHV)	Injector	SOFC running on propane with AOGR was experimentally examined and compared to a partial oxidation system.
Choi et al. [7]	1 kW	53.44% (LHV)	Blower	System performances with different system configurations were numerically examined and compared to the SOFC system without AOGR.
Torii et al. [1]	5 kW	69.2%	Blower	Effects of AOGR on system performance were investigated considering carbon deposition on a stack. The possibility of reducing operation cost with a AOGR system was also revealed.
Lee et al. [9]	30 W	-	-	Sensitivity analysis of diverse parameters on a SOFC system's performance with AOGR was conducted to predict key operating parameters and an optimal operating point was suggested.

Table 2. A literature summary of the SOFC analysis for design and optimization.

Authors	System Variables	System Performance	Method	Results
Lee et al. [9]	S/C ratio, stack temperature, AOGR ratio, CO_2 adsorbent	Power density, peak power, efficiency	Numerical individual parametric analysis	Suggested the optimal operating point for maximum efficiency (@ fuel cell temperature = 900 °C with S/C ratio > 3, maximum CO_2 capture, and minimum AOG recirculation)
Kalra et al. [11]	S/C ratio, fuel temperature, pressure, geometry of the SOFC	Power density	Numerical individual parametric analysis	Compared the effects of each parameter
Kupecki [12]	Mass flow rate, pressure ratio and polytrophic efficiency of air compressor, fuel flow rate of combustion chamber, pre-heater heat exchanger UA factor	Electrical efficiency, outlet temperature of SOFC, gas turbine, and combustion chamber	Numerical individual parametric analysis	Compared the effects of each parameter
Dhingra et al. [13]	Air and fuel utilization, oxygen to carbon ratio, S/C ratio, temperature of inlet cathode and pre-heater	System efficiency, stack efficiency, system exhaust temperature	Numerical individual and paired parametric analysis	Suggested the optimal operating point, the maximum system and stack efficiency (@ air utilization = 0.5, fuel utilization = 0.9, S/C ratio = 3)
Lee et al. [14]	Fuel utilization, S/C ratio, external reforming ratio	Electrical and thermal efficiency	Numerical individual parametric analysis	Compared the effects of each parameter

This study is based on the findings of our previous investigation. In the previous paper [7], the performance of an SOFC system with AOGR was numerically analyzed to determine the best system configuration. Based on the proposed system in [7], the objective of this paper is to determine the optimal operating conditions for actual operations. First, to determine the effects of operating parameters on the performance of the SOFC system, a model-based sensitivity analysis was conducted as described in Section 3.1. The control variables of the system were selected through sensitivity analysis. In Section 3.2, the available operating conditions are analyzed to achieve system reliability and target performance. Finally, three operating modes were proposed depending on the situation, and optimal operating points were suggested for each mode.

2. Methodology

Sensitivity analysis was carried out to determine the optimized operating conditions of an SOFC system. The lumped component model of an SOFC with AOGR, which was developed in the SIMULINK environment and validated in our previous paper [7], was used in this study. Detailed equations and explanations of the model were introduced in the previous paper; therefore, they are not repeated in this paper. Only the differences from the previous model are explained.

2.1. A System Configuration

In our previous paper, we evaluated the performance of the reference SOFC system and two different systems with AOGR. It was concluded that the AOGR #2 system, as shown in Figure 1, had the best performance among the three systems [7]. The optimal operating conditions for further analysis in the present study were defined using the AOGR #2 system. A summary of the system components is presented in Table 3. The flows of gases and energy in Figure 1 are described as follows: a mixture of inlet fuel (CH_4), steam, and recirculated AOG gains thermal energy at fuel preheater 1 and 2 from AOG and cathode off-gas (COG). The mixture then flows into an external steam reformer (ESR). After an electrochemical reaction between the reformed fuel and supplied air at an SOFC stack, the heat of COG was used in fuel preheater 2 and a steam generator. A certain amount of AOG, depending on the recirculation ratio (RR), resupplies to the inlet fuel flow by a recirculation blower. The rest of the AOG is used to generate thermal energy at the catalytic combustor (CC) and the heat is transferred to an air pre-heater by the flow of the catalytic combustor off-gas (CCOG). The remaining heat from the CCOG is recovered using a heat recovery heat exchanger (HR-HE). An additional air blower was employed for the catalytic combustor (CC) to prevent an excessive rise in its temperature. In Figure 1, the flows of recirculated AOG and COG are indicated by the orange and green lines, respectively. The blue line depicts the flow of CCOG.

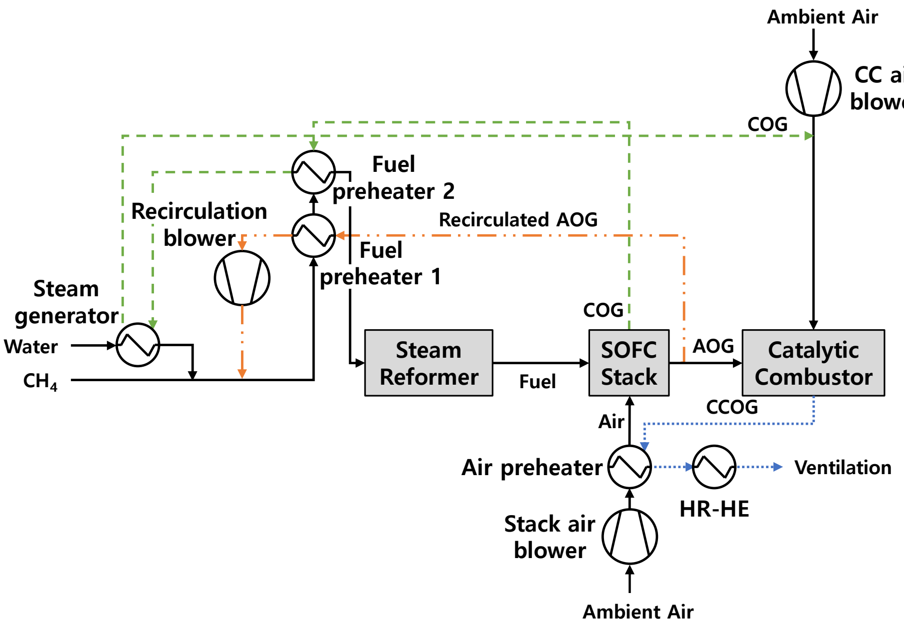

Figure 1. Schematic diagram of a solid oxide fuel cell (SOFC) system with anode off-gas recirculation (AOGR) (AOGR #2 system in ref. [7]).

Table 3. Descriptions of the main components.

Components	Descriptions	Ref. of Detailed Specifications
Stack	1 kW class planar SOFC A direct internal reforming stack Anode-supported cell type	Table 2 in the paper [7]
ESR	An adiabatic reformer A shell and tube type catalytic reformer	Table 4 in the paper [7]
CC	A Pt-catalyzed monolithic combustor	Table 6 in the paper [7]

2.2. Performance Factor

The fuel utilization factor (U_{fuel}) of the system was calculated using Equation (1). A mixture of supplied fuel (CH_4) and recirculated AOG flowed into the ESR. Methane (CH_4) is the only supplied fuel in this model, and the denominator in Equation (1) is calculated by considering recirculated AOG. The air utilization factor (U_{air}) can be defined using Equation (2).

$$U_{fuel} = \frac{J}{8F\dot{n}_{CH_4} + \left(8F\dot{n}_{CH_4} + 2F\dot{n}_{CO} + 2F\dot{n}_{H_2}\right)_{recycled}} \quad (1)$$

$$U_{air} = \frac{J}{4Fy_{O2}\dot{n}_{air}} \quad (2)$$

The net power of the system (P_{net}) is calculated by subtracting the power consumption of the balance of plant (BOP, $P_{FCBlower}, P_{CCBlower}, P_{RBlower}$) from the stack-generated power (P_{stack}), as shown in Equation (3). The electrical, thermal, and total efficiencies are described in Equations (4)–(6). The electrical efficiency of the system (η_{ele}) is defined as the ratio of the net power of the system to the chemical energy (LHV_{CH_4}) of the fuel supplied to the system. For the calculation of the thermal efficiency (η_{th}), the temperature of the system exhaust gas from the CC (T_{vent}) is assumed to be 393.15 K at the HR-HE.

$$P_{net} = P_{stack} - P_{FCBlower} - P_{CCBlower} - P_{RBlower} \quad (3)$$

$$\eta_{ele} = \frac{P_{net}}{\dot{m}_{CH_4}LHV_{CH_4}} \times 100 \quad (4)$$

$$\eta_{th} = \frac{c_{p,CCOG}\dot{m}_{CCOG}(T_{airPH,\text{o}} - T_{vent})}{\dot{m}_{CH_4}LHV_{CH_4}} \times 100 \quad (5)$$

$$\eta_{tot} = \eta_{ele} + \eta_{th} \quad (6)$$

2.3. Sensitivity Analysis Parameters

It is necessary to analyze the impact of the operating parameters on the system performance characteristics to determine the optimal operating conditions. There are lots of parameters that affect system performance. We selected three variables by considering the parameters that users can control during the actual operation. Consequently, the fuel flow rate (Q_{fuel}), air flow rate (Q_{air}), and RR were considered under two different load conditions. The changes in stack temperature (T_{stack}), recirculation blower temperature (T_{RB}), U_{fuel}, P_{net}, and system efficiencies (η_{elec}, η_{th}, and η_{tot}) were examined for the system performance characteristics.

The sensitivity of each parameter to the system performance characteristics was obtained from Equation (7). First, the system performance under base conditions (PC_{base}) was computed. Then, the system performance was calculated while varying a single operating variable (PC_{test}). When one parameter was changed, the others were kept constant at the base condition. Second, the change in the system performance characteristics from the results under the base conditions was calculated.

$$Sensitivity(\%) = \frac{PC_{test} - PC_{base}}{PC_{base}} \times 100 \quad (7)$$

The base conditions and variations for the sensitivity analysis are listed in Table 4. The sensitivity analysis was conducted with two different load conditions: current density of 0.3 A/cm^2 and 0.5 A/cm^2. The base conditions of the fuel and air flow rate are the values when U_{fuel} and U_{air} of the SOFC system without AOGR become 0.6 at either value of current density.

Table 4. Operating conditions for base condition and variation for sensitivity analysis.

Parameter		Values	Variation
Inlet fuel		CH_4	-
Operating pressure of the system (bar)		1.2	-
Operating current density (A/cm^2)		0.3, 0.5	-
Exhaust gas temperature (K)		393.15	-
S/C ratio at ESR		2.5	-
Ambient temperature (K)		298.15	-
Fuel flow rate (lpm)	j = 0.3 A/cm^2	3.20	2.00–6.00
	j = 0.5 A/cm^2	5.35	3.50–10.50

Air flow rate (lpm)	j = 0.3 A/cm^2	30.56	20.00–60.00
	j = 0.5 A/cm^2	50.94	30.00–100.00
Recirculation ratio		0.4	0–0.8

2.4. Restrictions and Target Performance of the SOFC System

For the thermal stability of system components such as a stack, recirculation blower, and catalytic combustor, there are restrictions on the operating temperature for each component. The desired operating temperature of an SOFC stack in the current study was set between 973.15–1123.15 K. For a recirculation blower and CC, it is generally known that they can withstand temperatures up to 1073.15 K and 1123.15 K, respectively [7,21]. The additional air flow rate to the CC was adjusted by the PI controller of a CC blower to keep the temperature of the CC below 1123.15 K.

The project, which provided funding for this research, is aimed at developing a highly efficient SOFC system with AOGR. Hence, the target fuel utilization factor and electrical efficiency of the SOFC system were above 0.7 and 45%, respectively. The restrictions and target performance are summarized in Table 5.

Table 5. Restrictions and target performances of the SOFC system in this study.

Parameter	**Values**
Desired operating temperature of an SOFC stack (K)	973.15–1123.15
Maximum temperature of a recirculation blower (K)	1073.15
Maximum temperature of a catalytic combustor (K)	1123.15
Target fuel utilization factor	0.7
Target electrical efficiency of the system (%)	45

3. Results and Discussion

3.1. The Result of Sensitivity Analysis

Figure 2a–c show the results of the sensitivity analysis of all performance characteristics with changes in the fuel flow rate, air flow rate, and recirculation ratio. Figure 2 intuitively explains the effect of each parameter on various performance characteristics. The results are similar regardless of the current density; therefore, Figure 2 only shows the results when the current density is 0.3 A/cm^2. The colors blue and yellow indicate positive and negative changes in each performance characteristic, respectively. The darker the color becomes, the larger the changes in the sensitivity values it indicates. White indicates the base condition. The grey-colored region is outside of the consideration conditions. The exact values of the sensitivity analysis are presented in Table 6.

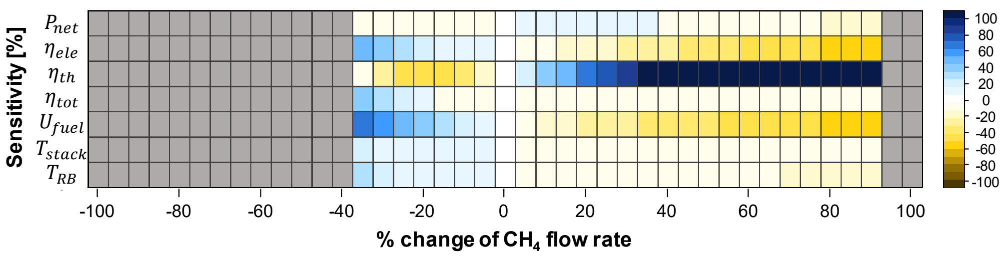

(**a**)

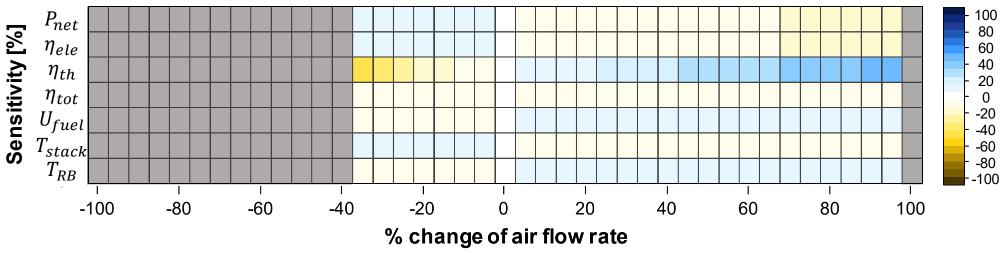

(b)

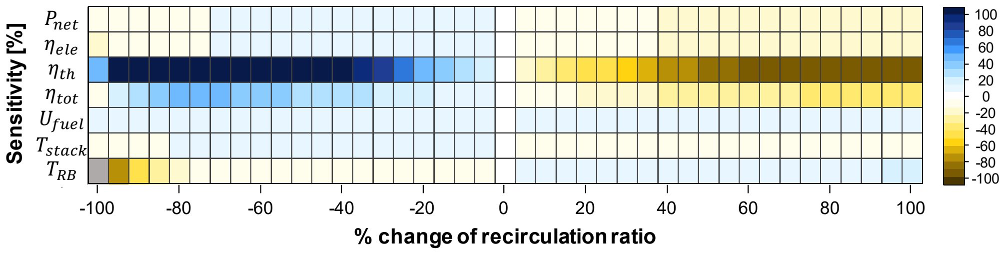

(c)

Figure 2. Sensitivity of (**a**) CH_4 flow rate, (**b**) air flow rate, and (**c**) recirculation ratio on performance characteristics.

Table 6. The result of sensitivity analysis of each parameter.

1. Sensitivity of CH_4 Flow Rate to System Performance (%)																						
Load	**$j = 0.3$ A/cm^2**											**$j = 0.5$ A/cm^2**										
% change	**−100**	**−80**	**−60**	**−40**	**−20**	**0**	**20**	**40**	**60**	**80**	**100**	**−100**	**−80**	**−60**	**−40**	**−20**	**0**	**20**	**40**	**60**	**80**	**100**
P_{net}	-	-	-	-	−8.5	0	2.9	−1.0	−6.1	−10.3	-	-	-	-	-	−12.1	0	2.8	−2.5	−7.6	−12.2	-
η_{elec}	-	-	-	-	14.6	0	−14.5	−28.9	−41.4	−50.6	-	-	-	-	-	9.7	0	−14.4	−30.3	−42.3	−51.2	-
η_{th}	-	-	-	-	−47.6	0	61.8	116	161.8	199	-	-	-	-	-	−47.6	0	57.2	107.5	149.7	182.4	-
η_{tot}	-	-	-	-	4.1	0	−1.8	−4.8	−7.5	−8.9	-	-	-	-	-	-1.4	0	−1.4	−5.4	−7.5	−8.9	-
U_{fuel}	-	-	-	-	33.1	0	−20.4	−33.4	−43.0	−50.5	-	-	-	-	-	33.6	0	−20.3	−33.6	−43.0	−50.1	-
T_{stack}	-	-	-	-	3.2	0	−0.8	−2.7	−4.8	−6.0	-	-	-	-	-	4.4	0	−0.9	−3.8	−5.6	−6.9	-
T_{RB}	-	-	-	-	6.4	0	−3.9	−7.3	−9.6	−10.6	-	-	-	-	-	7.8	0	−4.0	−8.8	−10.4	−11.4	-
2. Sensitivity of Air Flow Rate to System Performance (%)																						
Load	**$j = 0.3$ A/cm^2**											**$j = 0.5$ A/cm^2**										
% change	**−100**	**−80**	**−60**	**−40**	**−20**	**0**	**20**	**40**	**60**	**80**	**100**	**−100**	**−80**	**−60**	**−40**	**−20**	**0**	**20**	**40**	**60**	**80**	**100**
P_{net}	-	-	-	-	1.7	0	−2.9	−5.9	−8.7	−11.4	-	-	-	-	4.7	3.3	0	−3.2	−6.2	−9.2	−12.0	-
η_{elec}	-	-	-	-	1.7	0	−2.9	−5.9	−8.7	−11.4	-	-	-	-	4.7	3.3	0	−3.2	−6.2	−9.2	−12.0	-
η_{th}	-	-	-	-	−19.7	0	9.4	18.3	27.5	36.6	-	-	-	-	−33.6	−9.2	0	9.3	18.6	27.9	37.1	-
η_{tot}	-	-	-	-	−1.9	0	−0.9	−1.8	−2.6	−3.4	-	-	-	-	−2.3	1	0	−0.9	−1.7	−2.5	−3.1	-
U_{fuel}	-	-	-	-	0	0	0	0	0	0	-	-	-	-	0	0	0	0	0	0	0	-
T_{stack}	-	-	-	-	0.7	0	−1.2	−2.3	−3.2	−4.1	-	-	-	-	2.4	1.7	0	−1.4	−2.6	−3.6	−4.5	-
T_{RB}	-	-	-	-	−1.5	0	0.8	1	1	0.9	-	-	-	-	−1.7	−2.0	0	0.7	0.8	0.8	0.6	-
3. Sensitivity of Recirculation Ratio to System Performance (%)																						
Load	**$j = 0.3$ A/cm^2**											**$j = 0.5$ A/cm^2**										
% change	**−100**	**−80**	**−60**	**−40**	**−20**	**0**	**20**	**40**	**60**	**80**	**100**	**−100**	**−80**	**−60**	**−40**	**−20**	**0**	**20**	**40**	**60**	**80**	**100**
P_{net}	−9.9	−1.9	2.4	4.8	4.7	0	−4.7	−10.5	−15.2	−17.3	−16.8	−13.3	−2.9	1.6	4.3	4.8	0	−4.8	−11.3	−15.6	−16.9	−16.8
η_{elec}	−10.2	−1.9	2.4	4.8	4.7	0	−4.7	−10.5	−15.2	−17.3	−16.8	−13.3	−2.9	1.6	4.3	4.8	0	−4.8	−11.3	−15.6	−16.9	−16.8
η_{th}	45.3	257.5	200.8	116.8	49.7	0	−40.7	−72.4	−90.1	−97.7	−100.0	368.6	269.2	185.2	110.2	46.8	0	−38.5	−68.8	−84.2	−91.4	−96.3
η_{tot}	−0.9	41.7	35.2	23.5	12.1	0	−10.7	−20.8	−27.7	−30.7	−30.7	55.9	46.2	35	23.6	12.3	0	−10.9	−21.7	−28.1	−30.4	−31.2
U_{fuel}	8.2	5.4	3.1	1.4	0.4	0	0.5	2.3	4.1	4.9	4.7	8.6	5.5	3.1	1.4	0.4	0	0.5	2.4	3.7	4	3.8
T_{stack}	−5.4	0.3	1.5	2.2	2.3	0	−1.5	−2.2	−1.9	−1.2	−0.8	1.8	0.5	1	1.9	2.4	0	−1.5	−2.0	−1.6	−1.0	−0.6
T_{RB}	-	−11.5	−3.6	−1.6	−0.1	0	0.9	2.7	5.3	8.2	11		−12.1	−4.1	−1.8	−0.1	0	0.9	2.9	5.7	8.6	11.5

First, the effect of the fuel flow rate was examined as shown in Figure 2a. The base condition of the fuel flow rate was 3.2 lpm when U_{fuel} becomes 0.6 for the SOFC system without AOGR. The value was varied from 2.0–6.0 lpm, which corresponded to a change of −37.5% and 87.5% from the base condition. U_{fuel} became 0.9 and 0.3 when AOG was not recycled. Overall, the change in the fuel flow rate significantly affected U_{fuel}, η_{elec}, and η_{th}. The fuel flow rate obviously exhibited a negative correlation with U_{fuel}, T_{stack}, T_{RB}, and η_{elec}. The increased fuel flow rate to the stack enhanced the internal reforming reaction, leading to a reduction in T_{stack} and T_{RB}. On the other hand, P_{net} varied both positively and negatively as the fuel flow rate changed. This was because various factors were related to changes in P_{net}. Increased fuel flow to the stack can improve the stack performance by reducing the concentration overpotential loss when the fuel flow rate is low. However, this effect was cancelled out by the negative effect of the decreased stack temperature as the fuel flow rate increased [22]. For the efficiencies, a higher fuel flow rate negatively affected η_{elec}; however, it improved η_{th}. A slight increase in η_{th} at a low fuel flow rate was caused by a higher system temperature.

Second, the effect of the air flow rate was observed as presented in Figure 2b. The air flow rate was varied between −34.6% (20.0 lpm) and 96.3% (60.0 lpm) from the base flow rate (30.6 lpm), and they corresponded to U_{air} values of 0.9 and 0.3 when AOG was not recirculated. The impact of air flow rate variation on the performance characteristics was relatively small compared to the results in Figure 2a,c. Owing to the cooling effect of air, T_{stack} decreased slightly as the air flow rate increased. This yields to small decreases in P_{net} and η_{elec}. Meanwhile, the higher heat capacity of COG and CCOG resulting from the higher air flow rate enhanced the heat transfer amount at the steam generator and HR-HE. This increased T_{RB} and η_{th}.

Finally, the effect of the AOG recirculation ratio was examined. The base condition of the recirculation ratio was 0.4, and it was varied from 0 (no AOG recirculation) to 0.8. The percentage range is −100–100%. As shown in Figure 2c, the recirculation ratio had a strong influence on η_{th}. The mean fuel concentration at the CC caused by the enhanced recirculation ratio led to lower heat recovery at the HR-HE [6]. The increased AOG recirculation ratio also caused lower heat recovery at the fuel and air preheater, which led to a temperature decrease in the fuel and air supplied to the stack. Therefore, the T_{stack} varied within the range of ±5.4% from the temperature under the base condition. P_{net} enhanced gradually as the recirculation ratio increased; however, this effect was overcome with the fuel dilution problem at a higher recirculation ratio [7]. U_{fuel} varied only ±8.2% because the base value of the fuel flow rate was small. The effect of the recirculation ratio on U_{fuel} becomes noticeable at a higher fuel flow rate [6].

3.2. Optimization of Operating Condition

3.2.1. Desired Operating Conditions

Section 3.1 revealed that the sensitivity of the air flow rate to the system performance was weak compared to other operating parameters. Generally, the air flow rate is manipulated to control the stack temperature [4,22]. Therefore, the normal air flow rate was set as the value when U_{air} was 0.6 lpm. The PI controller adjusted the air flow rate when the stack temperature exceeded the available operating temperature, as shown in Table 5.

The purpose of this section is to determine the desired operating conditions that can satisfy the desired system performance. The target performance of the system was suggested in Section 2.4 and Table 5. U_{fuel} and η_{elec} were aimed to be simultaneously higher than 0.7 and 0.45, respectively. The changes in U_{fuel} and η_{elec} with varying fuel flow rates and recirculation ratios are shown in Figure 3a,b when the current density is 0.3 A/cm^2. The colored regions indicate the conditions that satisfy each target performance. When the fuel flow rate is low and the recirculation ratio is high, a significant concentration loss limits fuel cell performance. The results reveal that the system should be operated in a low fuel flow rate region (lower than 2.7 lpm) to meet the targeted U_{fuel} and η_{elec}. As shown in Figure 3, the impact of the recirculation ratio increases as the fuel flow rate increases.

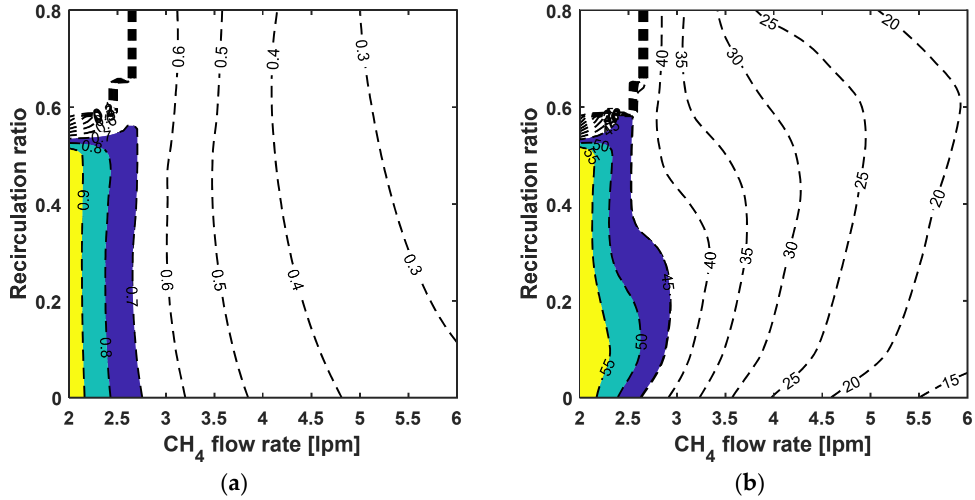

Figure 3. Changes of (**a**) fuel utilization factor (U_{fuel}) and (**b**) electrical efficiency (η_{elec}) with various fuel flow rates and recirculation ratios at current density of 0.3 A/cm².

The operating region where the result simultaneously satisfies both requirements can be the desired operating conditions, as shown in Figure 4a. The black region represents the available operating conditions. The desired operating region with different load conditions can be defined using the same process as in Figure 3. Figure 4b displays the desired operating region at 0.5 A/cm². At any operating point in the black area in Figure 4, the aimed performance (U_{fuel} > 0.7 and η_{elec} > 45%) can be guaranteed under certain load conditions. The optimal operating point can be determined in the desired operating region depending on the user requirements.

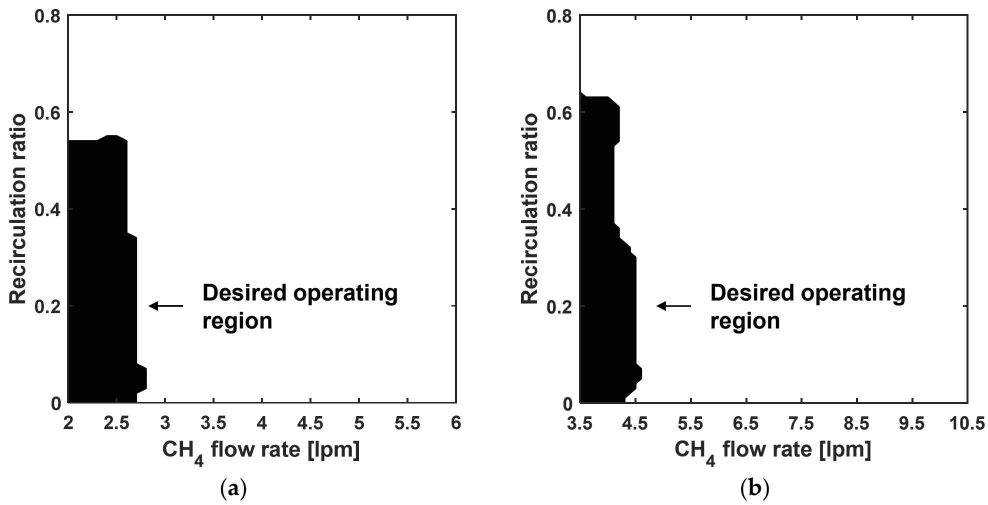

Figure 4. Desired operating conditions of the SOFC system with various fuel flow rates and recirculation ratios at operating current densities of (**a**) 0.3 A/cm² and (**b**) 0.5 A/cm².

3.2.2. Optimal Operating Point for Different Operating Scenario

Depending on the situation, users need to decide how to operate the SOFC system in the desired region, as suggested in Section 3.2.1. In this section, three scenarios are suggested: optimized electrical efficiency mode, peak power mode, and heat generation mode. The optimized electrical efficiency mode operates at the point when η_{elec} is maximized. Figure 5a,b present the change of η_{elec} when current densities are 0.3 A/cm² and

0.5 A/cm², respectively. Opaque areas represent the desired operating regions addressed in Section 3.2.1, and the red dot indicates the point with the maximum η_{elec}. In Figure 5a, the maximum η_{elec} was 59.57% when the fuel flow rate and RR were 2 lpm and 0.5, respectively. At that time, P_{net} was 771.5 W. In Figure 5b, as the fuel flow rate and RR reached 3.5 lpm and 0.6, respectively, η_{elec} reached a maximum of 55.25% and P_{net} became 1252.4 W.

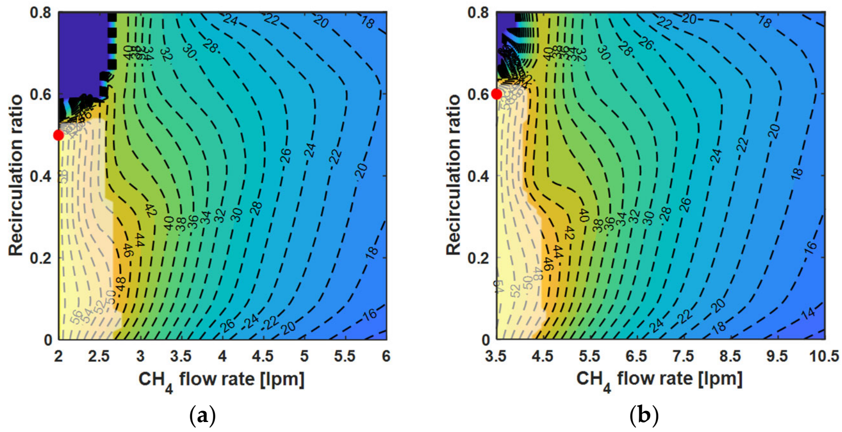

Figure 5. Change of electrical efficiency with various fuel flow rates and recirculation ratios at operating current densities of (**a**) 0.3 A/cm² and (**b**) 0.5 A/cm².

The second scenario was the peak power mode. This is the case when maximum power generation is required. The change in net power is shown in Figure 6a,b for each current density, and the red point represents the maximum point in the desired operating region. The maximum net power for each case was 851.2 W at 0.3 A/cm² and 1374.8 W at 0.5 A/cm². However, higher electrical power is required in some cases. The black points in each figure show the maximum power generated by the system. Maximum power of 863.7 W and 1398.5 W can be generated at 0.3 A/cm² and 0.5 A/cm², respectively. The system performance and operating conditions at the red and black points in Figure 6 are presented in Table 7.

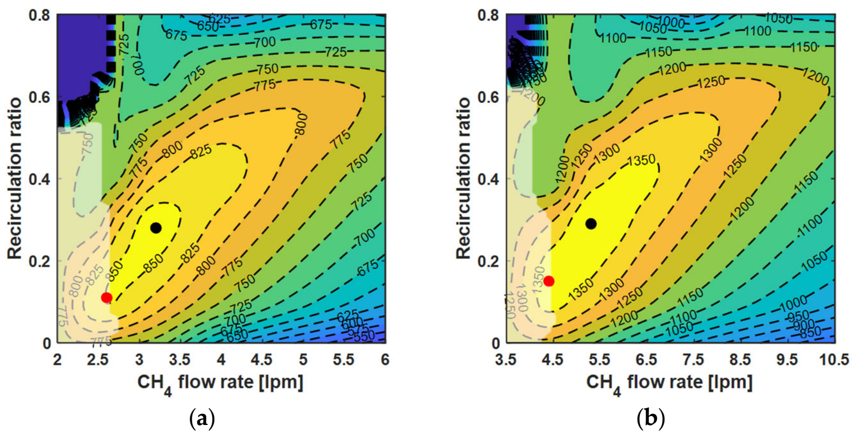

Figure 6. Change in net power with various fuel flow rates and recirculation ratios at operating current densities of (**a**) 0.3 A/cm² and (**b**) 0.5 A/cm².

Table 7. Operating conditions and the system performances when net power became maximized in Figure 6a,b.

Operating Conditions and the System Performances				
Load	**j = 0.3 A/cm²**		**j = 0.5 A/cm²**	
P_{net} **(W)**	**851.2 (●)**	**863.7 (●)**	**1374.8 (●)**	**1398.5 (●)**
Q_{CH_4} (lpm)	2.6	3.2	4.4	5.3
RR	0.11	0.28	0.15	0.29
η_{elec} (%)	50.4	41.7	48.1	40.7
η_{th} (%)	17.3	14.3	16.1	13.9
η_{tot} (%)	67.9	56.0	64.3	54.7
U_{fuel}	0.72	0.56	0.71	0.56

Finally, there can be a situation in which a large amount of thermal energy is required. For example, a smart farm sometimes needs higher heating energy and lower electrical energy, especially in winter. Figure 7 shows the change in thermal efficiency. As shown in both results, the AOGR system is disadvantageous in terms of thermal performance. Therefore, the maximum thermal efficiency can be obtained when RR is zero, and the fuel flow rate has the highest value in the desired operating region. The maximum η_{th} in Figure 7a was 28.7% and the fuel flow rate was 2.6 lpm. When the current density was 0.5 A/cm², the maximum η_{th} was 28.3% at a fuel flow rate of 4.2 lpm in Figure 7b. Additionally, higher thermal energy can be obtained at a higher fuel flow rate, if it is demanded.

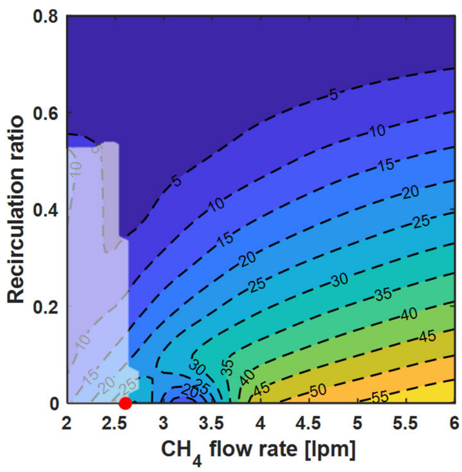

(**a**)

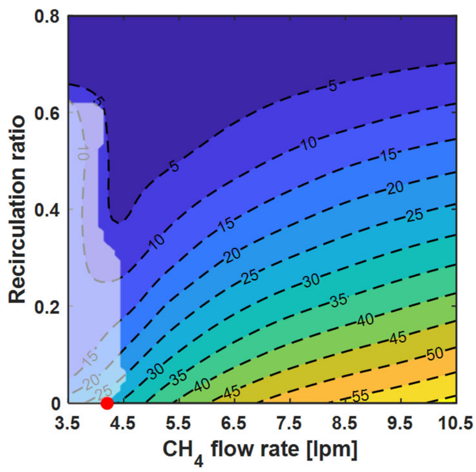

(**b**)

Figure 7. Change in thermal efficiency with various fuel flow rates and recirculation ratios at operating current densities of (**a**) 0.3 A/cm² and (**b**) 0.5 A/cm².

4. Conclusions

This study is a follow-up to our previous paper [7]. In the previous research, the layout of the SOFC system with AOGR was investigated, and a simulation model was developed for performance analysis. In this paper, the optimized operating conditions for the SOFC system with AOGR were suggested by utilizing the simulation model developed in ref. [7]. A sensitivity analysis of the operating parameters regarding system performance was conducted for the optimization. Through this process, we selected the control parameters for system operation. Second, the desired operating regions were found that satisfied the operating restrictions and target system performance. Finally, three operating scenarios were suggested, and optimized operating points were proposed considering each mode.

As the operating parameters for sensitivity analysis, Q_{fuel}, Q_{air}, and RR were selected. The effects of each parameter on the system performance (T_{stack}, T_{RB}, U_{fuel}, P_{net}, η_{elec}, η_{th}, and η_{tot}) were examined. Consequently, it was revealed that the impact of Q_{air} on the system was relatively small, while those of Q_{fuel} and RR were large. Based on the results, Q_{fuel} and RR were defined as control parameters. Meanwhile, the air flow rate was adjusted by a PI controller to regulate the temperature of the stack. Because of the thermal stability of the components, available temperature ranges exist during the operation. In addition, the project related to this study has a target system performance ($U_{fuel} > 0.7$ and $\eta_{elec} > 45\%$). Using the system performance map depicted in Figure 3 with various Q_{fuel} and RR values, the desired operating conditions, which can guarantee thermal safety of the system and the system performance, were proposed.

Additionally, optimized operating conditions are suggested for three operating scenarios: optimized electrical efficiency, peak power, and heat generation. Depending on the situation, the optimal points of Q_{fuel} and RR differed, and the AOGR system could be effective or not. When the current density was 0.3 A/cm^2, optimal operating conditions were obtained as follows: for the optimized electrical efficiency mode, a maximum η_{elec} of 59.57% was obtained at Q_{fuel} of 2 and RR of 0.5. For peak power mode and heat generation mode, P_{net} and η_{th} reached a maximum of 863.7 W and 27.8%, respectively, at Q_{fuel} of 2, RR of 0.5 and Q_{fuel} of 2.6, RR of 0. While operating SOFC systems, the requirements for electricity and heat can be diverse. Using the developed model and the process of this study, various optimized operating conditions can be derived for various cases, not only for the situation considered in this study.

Author Contributions: Conceptualization, E.-J.C.; simulation, E.-J.C., and S.Y.; investigation, E.-J.C.; writing, E.-J.C.; supervision, S.-M.L., and E.-J.C. All authors have read and agreed to the published version of the manuscript.

Funding: This work was supported by the Technology Innovation Program funded by the Korea Evaluation Institute of Industrial Technology (KEIT) and the Ministry of Trade, Industry & Energy (MOTIE) of the Republic of Korea (No. 20004963). This work was also funded by the Korea Institute of Energy Technology Evaluation and Planning (KETEP) and the Ministry of Trade, Industry & Energy (MOTIE) of the Republic of Korea (No. 20212020800050).

Institutional Review Board Statement: Not applicable.

Informed Consent Statement: Not applicable.

Conflicts of Interest: The authors declare no conflict of interest.

Nomenclature

c_p	specific heat capacity (J kg^{-1} K^{-1})
F	Faraday constant (C mole^{-1})
J	current (A)
j	current density (A cm^{-2})
$\dot{m}$	mass flow rate (kg s^{-1})
$\dot{n}$	molar flow rate (mole s^{-1})
P	power (W)
Q	volume flow rate (lpm)
T	temperature (K)
U	utilization factor
y	molar fraction
η	efficiency
Subscripts	
$elec$	electrical
th	thermal
tot	total
o	outlet

Abbreviations

AOG	anode off-gas
AOGR	anode off-gas recirculation
BOP	balance of plant
CC	catalytic combustor
COG	cathode off-gas
CCOG	catalytic combustor off-gas
ESR	external steam reformer
HR-HE	heat recovery heat exchanger
LHV	lower heating value
RB	recirculation blower
RR	recirculation ratio
S/C	steam to carbon
SOFC	solid oxide fuel cell

References

1. Torii, R.; Tachikawa, Y.; Sasaki, K.; Ito, K. Anode Gas Recirculation for Improving the Performance and Cost of a 5-KW Solid Oxide Fuel Cell System. *J. Power Sources* **2016**, *325*, 229–237, https://doi.org/10.1016/j.jpowsour.2016.06.045.
2. Xi, H.; Sun, J.; Tsourapas, V. A Control Oriented Low Order Dynamic Model for Planar SOFC Using Minimum Gibbs Free Energy Method. *J. Power Sources* **2007**, *165*, 253–266, https://doi.org/10.1016/j.jpowsour.2006.12.009.
3. Haberman, B.A.; Young, J.B. Three-Dimensional Simulation of Chemically Reacting Gas Flows in the Porous Support Structure of an Integrated-Planar Solid Oxide Fuel Cell. *Int. J. Heat Mass Transf.* **2004**, *47*, 3617–3629, https://doi.org/10.1016/j.ijheatmasstransfer.2004.04.010.
4. Li, S.; Zhan, C.; Yang, Y. Control System Based on Anode Offgas Recycle for Solid Oxide Fuel Cell System. *Math. Probl. Eng.* **2018**, *2018*, 1–16, https://doi.org/10.1155/2018/4198954.
5. Fardadi, M.; Mueller, F.; Jabbari, F. Feedback Control of Solid Oxide Fuel Cell Spatial Temperature Variation. *J. Power Sources* **2010**, *195*, 4222–4233, https://doi.org/10.1016/j.jpowsour.2009.12.111.
6. Peters, R.; Deja, R.; Engelbracht, M.; Frank, M.; Nguyen, V.N.; Blum, L.; Stolten, D. Efficiency Analysis of a Hydrogen-Fueled Solid Oxide Fuel Cell System with Anode Off-Gas Recirculation. *J. Power Sources* **2016**, *328*, 105–113, https://doi.org/10.1016/j.jpowsour.2016.08.002.
7. Choi, E.-J.; Yu, S.; Kim, J.-M.; Lee, S.-M. Model-Based System Performance Analysis of a Solid Oxide Fuel Cell System with Anode Off-Gas Recirculation. *Energies* **2021**, *14*, 3607, https://doi.org/10.3390/en14123607.
8. Wagner, P.H.; Van herle, J.; Schiffmann, J. Theoretical and Experimental Investigation of a Small-Scale, High-Speed, and Oil-Free Radial Anode Off-Gas Recirculation Fan for Solid Oxide Fuel Cell Systems. *J. Eng. Gas Turbines Power* **2020**, *142*, 041023, https://doi.org/10.1115/1.4045104.
9. Lee, T.S.; Chung, J.N.; Chen, Y.-C. Design and Optimization of a Combined Fuel Reforming and Solid Oxide Fuel Cell System with Anode Off-Gas Recycling. *Energy Convers. Manag.* **2011**, *52*, 3214–3226, https://doi.org/10.1016/j.enconman.2011.05.009.
10. Testa, E.; Maggiore, P.; Pace, L. Sensitivity Analysis for a PEM Fuel Cell Model Aimed to Optimization. *WSEAS Trans. Power Syst.* **2015**, *10*, 10.
11. Kalra, P.; Garg, R.K.; Kumar, A. Parametric Sensitivity Analysis for a Natural Gas Fueled High Temperature Tubular Solid Oxide Fuel Cell. *Heliyon* **2020**, *6*, e04450, https://doi.org/10.1016/j.heliyon.2020.e04450.
12. Kupecki, J. Sensitivity Analysis of Main Parameters of Pressurized SOFC Hybrid System. *J. Power Technol.* **2019**, *99*, 115.
13. Dhingra, H.; Peppley, B.A. Sensitivity Analysis of a 1 KW Diesel-Fuelled SOFC Generator: A Single and Paired-Variable Study. *J. Power Sources* **2013**, *239*, 527–537, https://doi.org/10.1016/j.jpowsour.2013.03.107.
14. Lee, K.; Kang, S.; Ahn, K.-Y. Development of a Highly Efficient Solid Oxide Fuel Cell System. *Appl. Energy* **2017**, *205*, 822–833, https://doi.org/10.1016/j.apenergy.2017.08.070.
15. Powell, M.; Meinhardt, K.; Sprenkle, V.; Chick, L.; McVay, G. Demonstration of a Highly Efficient Solid Oxide Fuel Cell Power System Using Adiabatic Steam Reforming and Anode Gas Recirculation. *J. Power Sources* **2012**, *205*, 377–384, https://doi.org/10.1016/j.jpowsour.2012.01.098.
16. Koo, T.; Kim, Y.S.; Lee, D.; Yu, S.; Lee, Y.D. System Simulation and Exergetic Analysis of Solid Oxide Fuel Cell Power Generation System with Cascade Configuration. *Energy* **2021**, *214*, 119087, https://doi.org/10.1016/j.energy.2020.119087.
17. Wagner, P.H.; Wuillemin, Z.; Constantin, D.; Diethelm, S.; Van herle, J.; Schiffmann, J. Experimental Characterization of a Solid Oxide Fuel Cell Coupled to a Steam-Driven Micro Anode Off-Gas Recirculation Fan. *Appl. Energy* **2020**, *262*, 114219, https://doi.org/10.1016/j.apenergy.2019.114219.
18. Baba, S.; Takahashi, S.; Kobayashi, N.; Hirano, S. Performance of Anodic Recirculation by a Variable Flow Ejector for a Solid Oxide Fuel Cell System under Partial Loads. *Int. J. Hydrogen Energy* **2020**, *45*, 10039–10049, https://doi.org/10.1016/j.ijhydene.2020.01.191.

19. Tanaka, Y.; Sato, K.; Yamamoto, A.; Kato, T. Development of Anode Off-Gas Recycle Blowers for High Efficiency SOFC Systems. *ECS Trans.* **2013**, *57*, 443–450, https://doi.org/10.1149/05701.0443ecst.
20. Dietrich, R.-U.; Lindermeir, A.; Immisch, C.; Spieker, C.; Spitta, C.; Stenger, S.; Leithner, R.; Kuster, T.; Oberland, A. SOFC System Using a Hot Gas Ejector for Offgas Recycling for High Efficient Power Generation from Propane. *ECS Trans.* **2013**, *57*, 171–184, https://doi.org/10.1149/05701.0171ecst.
21. Kong, Q.; Yin, Y.; Xue, B.; Jin, Y.; Feng, W.; Chen, Z.-G.; Su, S.; Sun, C. Improved Catalytic Combustion of Methane Using CuO Nanobelts with Predominantly (001) Surfaces. *Beilstein J. Nanotechnol.* **2018**, *9*, 2526–2532, https://doi.org/10.3762/bjnano.9.235.
22. Jiang, W.; Fang, R.; Khan, J.A.; Dougal, R.A. Parameter Setting and Analysis of a Dynamic Tubular SOFC Model. *J. Power Sources* **2006**, *162*, 316–326, https://doi.org/10.1016/j.jpowsour.2006.06.086.